Plasma sheath model and ion energy distribution for all radio frequencies

Theodoros Panagopoulos and Demetre J. Economou[a)]
Plasma Processing Laboratory, Department of Chemical Engineering, University of Houston, Houston, Texas 77204-4792

(Received 24 September 1998; accepted for publication 31 December 1998)

The spatiotemporal structure of the sheath and the ion energy distribution (IED) at the electrode of a collisionless electropositive glow discharge were studied with a model that is valid for arbitrary radio frequencies (rf). The model is based on the work of P. A. Miller and M. E. Riley [J. Appl. Phys. **82**, 3689 (1997)] and uses an effective electric field to which the heavy ions respond. Given the plasma density and electron temperature at the sheath edge, and the waveform of either the potential or total current across the sheath, the spatial and/or temporal profiles of the following quantities were obtained: sheath thickness and capacitance, electron and ion densities, potential, and individual components of the current. An analytic expression for the energy split of the IED function was also obtained. The product $\omega\tau_i$ of applied radian frequency ω and ion transit time τ_i is a critical parameter for describing the sheath dynamics.
[S0021-8979(99)02207-0]

I. INTRODUCTION

A. Sheath dynamics

Understanding the dynamics of the sheath formed over a radio frequency (rf) powered electrode immersed in a plasma is important from both the fundamental and practical points of view. The sheath dynamics controls the energy and angular distribution of ions bombarding the electrode, which in turn affect the surface reaction rate and wall profile of microscopic features etched into wafers resting on the electrode. High density plasma reactors have the advantage of quasi-independent control of plasma density and ion bombardment energy.[1] This is achieved by separating plasma production from the bias voltage applied to the substrate electrode. In addition, the small Debye length (thin sheath) and low pressure (long ion mean free path) result in collision-free sheath which minimizes the ion angular distribution (IAD). However, even in the absence of collisions, an ion energy distribution (IED) at the substrate electrode could result due to the sheath potential oscillation, even if ions injected at the sheath edge were monoenergetic.

The critical parameter that controls ion modulation in rf sheaths is $\omega\tau_i$, where ω is the frequency of the applied field, and τ_i is the ion transit time through the sheath. The ion transit time can be estimated by assuming a collisionless Child–Langmuir (dc) sheath, and neglecting the velocity of ions (Bohm velocity) entering at the sheath edge. The result is[2]

$$\tau_i = 3s\sqrt{m_i/(2eV_{\mathrm{sh}})}, \tag{1}$$

where s is the sheath thickness, m_i is the ion mass, V_{sh} is the sheath voltage, and e is the elementary charge. For an rf sheath, the sheath thickness and voltage across the sheath could be approximated by the corresponding time-average values when using Eq. (1). When $\omega\tau_i \ll 1$, ions traverse the sheath in a short time compared to the field oscillations. Under this condition, an ion traversing the sheath experiences the sheath voltage prevailing at the time the ion entered the sheath. In the absence of collisions, the IED function will reflect the variation of the sheath voltage with time. This quasi-steady-state condition of $\omega\tau_i \ll 1$ is satisfied for low rf frequencies or short ion transit times, i.e., thin sheaths (low sheath voltage and/or small Debye length), or ions of small mass. At the other extreme of $\omega\tau_i \gg 1$, ions experience many field oscillations while in transit through the sheath. Ions will then respond to the time-average sheath potential, and the IED function should exhibit a single peak.

The two extreme conditions discussed above are more amenable to analysis since, in both cases, the sheath can be described as a dc sheath; actually a series of dc sheaths at the different moments in time during the rf cycle when $\omega\tau_i \ll 1$, and a dc sheath at the time-average voltage when $\omega\tau_i \gg 1$. The most difficult situation to analyze is when $\omega\tau_i \sim 1$.

The literature on rf sheaths is voluminous. Both fluid[3–7] and kinetic (e.g., Monte Carlo)[8–12] simulations have been reported. One of the most important results of such simulations is the IED. Most models are for either the low or the high frequency regimes. Monte Carlo simulations have been performed in the intermediate frequency regime.[11,12]

Lieberman's model[3] applies to high rf frequencies ($\omega\tau_i \gg 1$) for which ions respond only to the time-average electric field. Lieberman assumed a sinusoidal waveform for the total rf current passing through the sheath. The ion cloud was not modulated in time, and ions entered the sheath with the Bohm velocity. A sharp (step function) moving front was assumed for the electrons inside the sheath with the electron density equal to the ion density on the plasma side of the front, and zero on the wall side of the front. There was no electron particle current to the wall, i.e., the dc component of the discharge current was not required to vanish. Godyak and Sternberg[4] used a sheath model similar to that of Lieberman

[a)]Electronic mail: economou@uh.edu

but they took into account the electron and ion conduction currents in the sheath. On the other hand, the sheath model of Metze *et al.*[5] is applicable to the low frequency regime ($\omega\tau_i \ll 1$) for which ions are able to respond to the instantaneous voltage across the sheath.

However, there are many cases of plasma density and rf bias voltage encountered in high density plasma reactors for which neither the low nor the high frequency sheath models are applicable. A sheath model developed by Miller and Riley[6] bridges the gap between the low and high frequency regimes. The main feature of this model is to introduce a damped potential to which ions respond. Actually this damped (or effective) potential was used before for reactor scale fluid plasma simulations,[13–15] but had not been used for sheath simulations. Miller and Riley made the *ad hoc* assumption that the damped potential has the same spatial dependence as the actual potential. They used their model to calculate the electrical characteristics of a high density plasma reactor. They also reported the IED derived from their model but did not study the effect of process variables on the IED. Finally, Miller and Riley did not calculate the spatiotemporal profiles of important sheath variables (sheath thickness, potential, electron, and ion densities).

B. Ion energy distribution

Benoit-Cattin and Bernard[16] analytically calculated the IED and the energy dispersion (peak separation) ΔE_i for the case $\omega\tau_i \gg 1$. They assumed a constant sheath width, uniform electric field within the sheath, a sinusoidal sheath voltage $V_{sh}(t) = V_{dc} + V_{ac}\sin(\omega t)$ and a zero initial ion velocity at the plasma-sheath boundary. The derived expressions for the energy dispersion and the IED function are

$$\Delta E_i = \left(\frac{8eV_{ac}}{3\omega s}\right)\left(\frac{2eV_{dc}}{m_i}\right)^{1/2}, \tag{2}$$

$$f(E_i) = \left(\frac{2N_s}{\omega \Delta E_i}\right)\left[1 - \left(\frac{4}{\Delta E_i^2}\right)(E_i - eV_{dc})^2\right]^{-1/2}, \tag{3}$$

where s is the constant sheath thickness, and N_s the number of ions entering the sheath per unit time.

Tsui[10] numerically integrated the ion equations of motion and obtained IED profiles assuming constant sheath width, a linearly varying electric field within the sheath, a sinusoidal sheath voltage, and a Maxwellian ion velocity distribution at the plasma-sheath boundary. Okamoto and Tamagawa[17] calculated analytically the energy dispersion ΔE_i for the high frequency regime to find

$$\Delta E_i \approx \frac{8eV_{ac}}{\omega\tau_i}, \tag{4}$$

which is identical to Eq. (2) when Eq. (1) is taken into account. They also verified experimentally (for frequencies from 20 to 80 MHz) that the energy dispersion scales inversely with frequency and the square root of ion mass [see also Eq. (2)]. Coburn and Kay[18] extended the ion mass range studied by Okamoto and Tamagawa and also showed that $\Delta E_i \propto m_i^{-1/2}$. A review of ion energy distributions in capacitively coupled rf electrodes can be found elsewhere.[2] The above expressions related to the IED function are valid for high frequencies, $\omega\tau_i \gg 1$. We are not aware of published expressions that are valid for arbitrary values of $\omega\tau_i$.

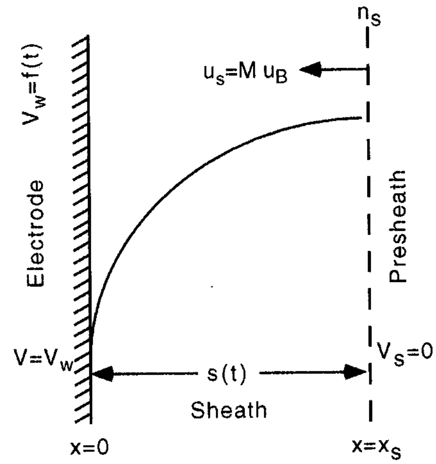

FIG. 1. Schematic of a sheath adjacent a biased electrode where a periodic voltage is being applied. The time-dependent sheath thickness is $s(t)$.

In the present work, the model of Miller and Riley[6] was adopted to calculate the spatial and/or temporal profiles of important sheath quantities such as: sheath thickness and capacitance, electron and ion densities, potential, and individual components of the current. Knowing the sheath thickness allows one to calculate the actual ion transit time. By solving the sheath equations numerically it was found that, indeed, the damped potential has the same spatial dependence as the actual potential. The ion energy distribution function for arbitrary values of $\omega\tau_i$ was also obtained, and an analytic expression for the peak separation of the IED was derived.

II. MODEL FORMULATION

A. Model equations

A model was developed for a collisionless sheath in an electropositive plasma containing only one type of positive ions (Fig. 1). Extension to multiple positive ion species is straightforward. The model may be applicable to electronegative plasmas as well in cases for which the negative ion density is essentially zero at the sheath edge. For example, electronegative discharges often separate into a core containing the negative ions, and a periphery which is essentially devoid of negative ions (p. 324 of Ref. 1). This depends on the ratio of electron to negative ion density and the ratio of electron to negative ion temperature.[19]

The potential distribution within the sheath is described by Poisson's equation

$$\nabla^2 V = -\frac{\rho}{\epsilon_0}, \tag{5}$$

where V is the instantaneous potential, ρ is the charge density, and ϵ_0 is the permittivity of free space. The charge density is given by

$$\rho = e(Zn_i - n_e), \tag{6}$$

where Z is the relative charge of the positive ion in units of e, n_i is the ion density, and n_e is the electron density. For simplicity, it was assumed that $Z=1$.

The electrons were assumed to be in Boltzmann equilibrium (p. 40 in Ref. 1) with the electron density given by

$$n_e(x,t)=n_e(x_s,t)\exp\left(\frac{V(x,t)-V(x_s,t)}{T_e}\right), \tag{7}$$

where x_s denotes the sheath edge (Fig. 1). In the above expression, T_e is the electron temperature in Volts. Use of T_e implicitly assumes that electrons have a Maxwellian energy distribution. It was also assumed that the electron temperature is constant in time and space. Furthermore, assuming collisionless sheath, the ion density n_i and ion fluid velocity u_i are described by the following conservation equations

$$n_i(x,t)u_i(x,t)=n_i(x_s,t)u_i(x_s,t), \tag{8}$$

$$\tfrac{1}{2}m_iu_i^2(x,t)+e\overline{V}(x,t)=\tfrac{1}{2}m_iu_i^2(x_s,t)+e\overline{V}(x_s,t), \tag{9}$$

Equation (8) assumes adiabatic ions, an assumption made in Ref. 6 as well. Combining these two equations, the ion density can be expressed as

$$n_i(x,t)=n_i(x_s,t)\left(1-\frac{2e}{m_iu_i^2(x_s,t)}(\overline{V}(x,t)-\overline{V}(x_s,t))\right)^{-1/2}. \tag{10}$$

Ions do not respond to the actual potential but rather to an effective damped potential (or field) $\overline{V}$

$$\frac{\partial\overline{V}(x,t)}{\partial t}=-\frac{[\overline{V}(x,t)-V(x,t)]}{\tau_i}, \tag{11}$$

where τ_i is a time constant that controls the amount of ''averaging'' involved in $\overline{V}$. This time constant should be the ion transit time through the sheath. For an unbiased sheath, the ion transit time is equal to the inverse of the ion plasma frequency based on the plasma density at the sheath edge.

$$\tau_i=\frac{1}{\omega_{pi}}, \tag{12}$$

where ω_{pi} is

$$\omega_{pi}=\left(\frac{e^2n_s}{\epsilon_0m_i}\right)^{1/2}. \tag{13}$$

This is the ratio of the Bohm velocity of ions to the electron Debye length.

Equations (5)–(11) may be combined to yield the following two equations which describe the sheath dynamics,

$$\nabla^2V=-\frac{en_s}{\epsilon_0}\left[\left(1-\frac{2\overline{V}}{M^2T_e}\right)^{-1/2}-\exp\left(\frac{V}{T_e}\right)\right], \tag{14}$$

$$\frac{\partial\overline{V}(x,t)}{\partial t}=-\frac{[\overline{V}(x,t)-V(x,t)]}{\tau_i}. \tag{15}$$

for which the boundary conditions [Eqs. (16) and (17)] have been taken into account.

B. Boundary conditions

Ions entering the sheath from the bulk plasma have velocities equal to the Bohm velocity

$$u_B=M\left(\frac{eT_e}{m_i}\right)^{1/2}, \tag{16}$$

where M is the Mach number and $M\geqslant 1$. The Bohm criterion guarantees that the ion density within the sheath is always greater than the electron density. Whenever there was a violation of this condition in the sheath, the Mach number was increased[6] so that the ion density was always higher than the electron density. The potential at the sheath-presheath boundary was set equal to zero.

$$\text{At}\quad x=x_s(\text{sheath-presheath interface}),\quad V=0. \tag{17}$$

This means that the wall voltage V_w is identical to the sheath voltage. The latter is given by

$$\text{At}\quad x=0(\text{electrode}),\quad V_w(t)=f(t), \tag{18}$$

where $f(t)$ can be any periodic function. It was assumed that $f(t)$ is given by the following expression:

$$f(t)=V_{\mathrm{dc}}+\sum_j V_{\mathrm{ac}_j}\cos(j\omega t+\theta_j), \tag{19}$$

The electric field at the sheath-presheath boundary was set equal to E_s.

$$\frac{\partial V}{\partial x}=-E_s. \tag{20}$$

The value of E_s suggested by Riley[20] was used,

$$E_s=-\frac{T_e}{\lambda_i}\log(\epsilon^2), \tag{21}$$

where ϵ is the ratio of the electron Debye length to the ion mean free path,

$$\epsilon=\frac{\lambda_{\mathrm{De}}}{\lambda_i}. \tag{22}$$

Finally, the electron temperature and the ion (equal to the electron) density were both specified at the sheath-presheath interface.

$$\text{At } x=x_s(\text{sheath-presheath interface})\,T_e \text{ and } n_s \text{ are given.} \tag{23}$$

The final sheath equations consist of a two-point boundary value problem [Eq. (14)] coupled with an ordinary differential equation [Eq. (15)], and the boundary conditions, Eqs. (16)–(23).

Solving Eq. (15) at the electrode, using Eqs. (18) and (19), one obtains the following analytical solution for the damped potential at the wall, $\overline{V}_w$

$$\overline{V}_w(t)=V_{\mathrm{dc}}+\sum_j\frac{V_{\mathrm{ac}_j}}{1+(j\omega\tau_i)^2}[\cos(j\omega t+\theta_j) +(j\omega\tau_i)\sin(j\omega t+\theta_j)], \tag{24}$$

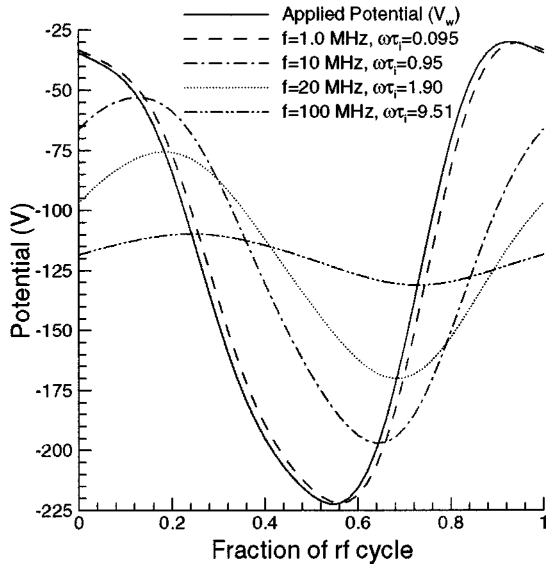

FIG. 2. Solid line shows the harmonic potential applied to the electrode, which is also equal to the sheath potential. This was taken to approximate the measured potential shown in Fig. 13 of Ref. 6. The damped potential $\overline{V}$ calculated by using Eq. (15) is shown as broken lines for different values of $\omega\,\tau_i$.

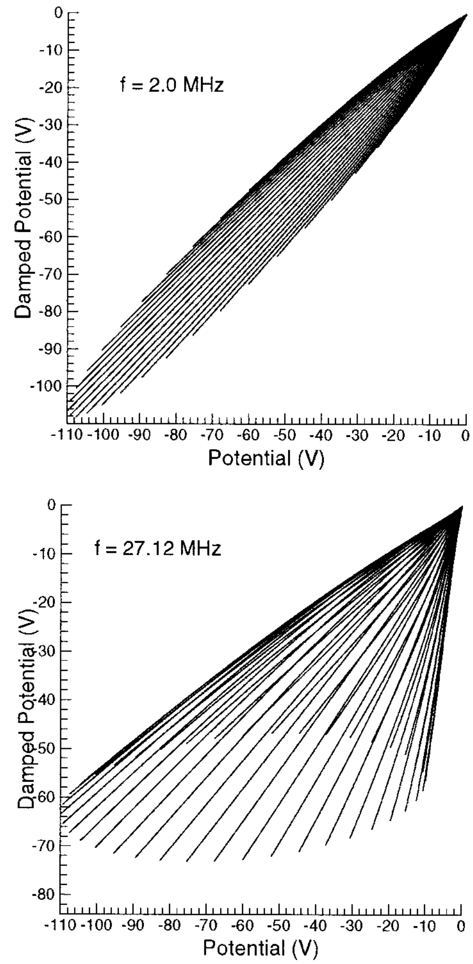

FIG. 3. Relationship between damped potential $\overline{V}$ to real potential V as calculated numerically. Each line corresponds to a specific time in the rf cycle and represents values of the potentials across the thickness of the sheath at that time. Point (0,0) corresponds to the sheath-presheath boundary while the other end of the line represents the electrode.

The potentials at the wall (V_w and $\overline{V}_w$) are plotted as a function of time for a number of different frequencies in Fig. 2. For this particular case, the potential applied at the wall was taken to approximate the experimental waveform measured by Miller and Riley shown in Fig. 13 of their paper.[6] When $\omega\tau_i$ is much less than unity, $\overline{V}_w$ almost coincides with V_w. Increasing $\omega\tau_i$ reduces the amplitude of $\overline{V}_w$ and introduces a phase shift. For large values of $\omega\tau_i$, the modulation of $\overline{V}_w$ is negligible.

The sheath thickness is not known *a priori*. This is why three boundary conditions [Eqs. (17), (18), and (20)] are required for solving Poisson's equation. The extra boundary condition serves to fix the sheath thickness such that the value of the electric field at the sheath-presheath boundary is E_s. The Poisson Eq. (14) was discretized by a fourth order finite difference stencil and the resulting system of equations was solved simultaneously with Eq. (15) using LSODE.[21] The solution provided the spatial and/or temporal profiles of sheath quantities such as thickness, potential, V, damped potential, $\overline{V}$, and electron and ion densities. In Fig. 3, $\overline{V}$ is plotted as a function of V for two different frequencies (2.0 and 27.12 MHz). The electron temperature was set at 3 eV, and the plasma density at the sheath edge was $n_s = 6\times10^{16}\,\mathrm{m}^{-3}$. These base case values were kept unchanged unless noted otherwise. The sheath-presheath boundary is located at point (0, 0) while the other endpoint of each line corresponds to the electrode, i.e., each line spans the whole sheath for a particular point in time during an rf cycle. The relationship between the two potentials is nearly linear, $\overline{V} = \alpha(t)V$, an assumption that was made *ad hoc* by Miller and Riley.[6] Based on this observation, the following semianalytic model was derived as a simplification of the initially posed sheath problem.

III. SEMIANALYTIC SHEATH MODEL

The time-dependent proportionality constant between the damped potential and the actual potential can be derived from the values of the potentials at the electrode [Eqs. (18), (19), and (24)].

$$\alpha(t) = \frac{\overline{V}_w}{V_w} = \frac{V_{\mathrm{dc}} + \sum_j \dfrac{V_{\mathrm{ac}_j}}{1+(j\omega\tau_i)^2}[\cos(j\omega t+\theta_j) + (j\omega\tau_i)\sin(j\omega t+\theta_j)]}{V_{\mathrm{dc}} + \sum_j V_{\mathrm{ac}_j}\cos(j\omega t+\theta_j)}. \tag{25}$$

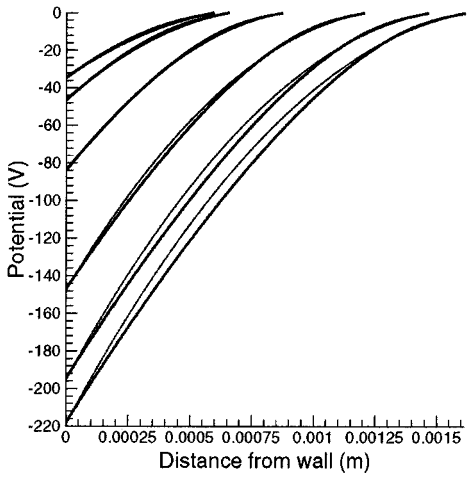

FIG. 4. Potential in the sheath as a function of space and time. Thick lines: numerical solution. Thin lines: semianalytic solution. The frequency was 10 MHz, the electron temperature was 3 eV, and the plasma density at the sheath edge was $n_s = 6\times 10^{16}\ \mathrm{m}^{-3}$.

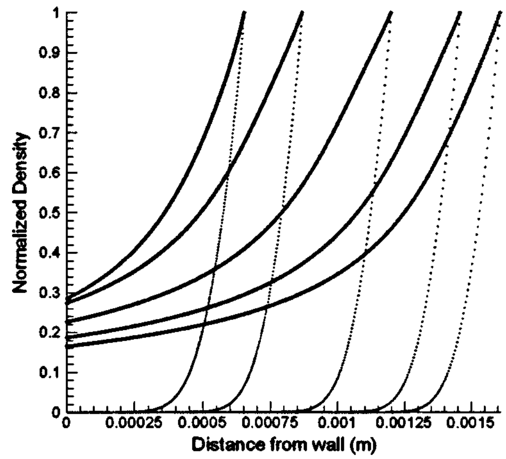

FIG. 5. Normalized ion (solid lines) and electron (dotted lines) densities (to their value at the sheath-presheath boundary) as a function of time and space in the sheath. Conditions as in Fig. 4.

Using Eq. (25), the sheath equations [Eqs. (14) and (15)] can be decoupled, and the Poisson equation can be solved independently

$$\frac{\partial^2 V}{\partial x^2} = -\frac{en_s}{\epsilon_0}\left[\left(1-\frac{2\alpha(t)}{M^2T_e}\cdot V\right)^{-1/2} - \exp\left(\frac{V}{T_e}\right)\right]. \tag{26}$$

Multiplying each side of Eq. (26) by $\partial V/\partial x$ and integrating over x, the electric field in the sheath is derived as

$$E(x,t) = -\left(E_s^2 + \frac{2en_sT_e}{\epsilon_0}\left\{\frac{M^2}{\alpha(t)}\left[\left(1-\frac{2\alpha(t)}{M^2T_e}V\right)^{1/2} - 1\right] + \left[\exp\left(\frac{V}{T_e}\right) - 1\right]\right\}\right)^{1/2}. \tag{27}$$

Figure 4 shows a comparison between the spatiotemporal profile of the potential calculated numerically by solving Eqs. (14) and (15), and that calculated analytically using Eq. (27), for a frequency of 10 MHz. The correspondence between the two is quite good. Similar results were obtained for both smaller and larger frequencies.

Once the potential profiles are known, the ion and electron density profiles in the sheath can be found as [see Eqs. (7) and (10)],

$$n_i = n_s\left(1-\frac{2\overline{V}}{M^2T_e}\right)^{-1/2}, \quad n_e = n_s \exp\left(\frac{V}{T_e}\right). \tag{28}$$

The ion density (Fig. 5) drops substantially near the sheath-presheath boundary at a rate that depends on the value of the electric field at that point, E_s. The ion density is always higher than the electron density within the sheath. When the sheath thickness reaches its minimum value, there is a substantial electron particle current to the electrode. As the electrode potential becomes more negative, electrons are repelled, and the electron density at the wall becomes extremely low.

Figure 6 shows the time dependence of the sheath thickness for the base case conditions. The sheath thickness calculated by the Child law formula (assuming a quasi-steady-state sheath) is also superimposed on the figure. As expected, the sheath thickness responds to the waveform of the sheath potential (Fig. 2, solid line). When the (negative) sheath potential is minimum (maximum) the sheath thickness is maximum (minimum).

A question arises as to what value to use for the ion transit time in Eq. (15). Miller and Riley[6] used the reciprocal of the ion plasma frequency [Eq. (12)] and this is what we have also used up to this point. Another approach would be to calculate the ion transit time iteratively. One would then assume an ion transit time, solve the sheath equations, integrate the equation of motion for the ions to find the actual transit time, and then iterate this procedure until the assumed and calculated ion transit times agree to within a specified tolerance. Figure 6 also compares the sheath thickness as a function of time calculated using the reciprocal of the ion plasma frequency (solid line) and the iterative procedure just described for determining the ion transit time (dotted line). Conditions were at their base case values. Using the ion

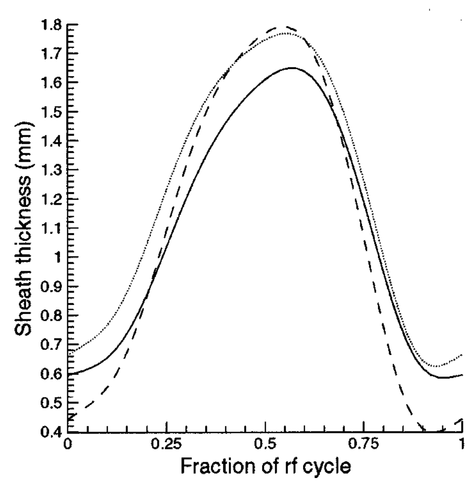

FIG. 6. Sheath thickness as a function of time for the conditions of Fig. 4 (solid line). The sheath thickness resulting from the Child Law model is also shown for comparison (dashed line). Dotted line was found by using a self-consistent calculation of the ion transit time.

plasma frequency to calculate the ion transit time does not introduce considerable error in calculating the time-dependent sheath thickness. However, an accurate value of the ion transit time is necessary to compute the correct ion energy distribution function, as shown below.

IV. ION ENERGY DISTRIBUTION

As described above, the damped potential $\overline{V}$ describes the motion of the heavy ions through the sheath. The potential that ions experience in their journey through the sheath is the difference of the damped potential between the wall and the sheath-presheath boundary. Because $\overline{V}$ is always zero at the sheath-presheath boundary, the sheath potential ions experience is equal to the value of the damped potential at the wall ($\overline{V}_w$).

The most critical parameter that controls ion motion in the (collisionless) sheath is $\omega\tau_i$. At low frequencies $\omega\tau_i \ll 1$ and $\overline{V}_w = V_w \Rightarrow \alpha(t)=1$ since the variation of the electric field is slow and ions respond to the instantaneous changes of the field. As a result, V and $\overline{V}$ coincide. At high frequencies $\omega\tau_i \gg 1$, Eq. (24) reduces to,

$$\overline{V}_w = V_{dc} + \sum_j \frac{V_{ac_j}\sin(j\omega t+\theta_j)}{(j\omega\tau_i)}. \tag{29}$$

The higher the value of the critical parameter $\omega\tau_i$, the smaller the amplitude of the oscillations of $\overline{V}_w$. For the sake of simplicity, V_w will now be assumed sinusoidal,

$$V_w(t) = V_{dc} + V_{ac}\sin(\omega t). \tag{30}$$

Knowing the time-dependent sheath potential (here the wall potential, V_w), the damped potential, $\overline{V}_w$, can be found readily by integrating Eq. (15). The minimum and maximum values of energy of ions striking the electrode correspond to the minimum and maximum values of $\overline{V}_w$ which are found by

$$\frac{d\overline{V}_w}{dt} = 0 \Rightarrow (\omega\tau_i)\sin(\omega t) + \cos(\omega t) = 0. \tag{31}$$

Solution of Eq. (31) gives the times at which the damped sheath potential reaches its maximum and minimum values

$$t_{max} = \frac{1}{\omega}\left[\tan^{-1}\left(-\frac{1}{\omega\tau_i}\right) + \pi\right], \tag{32a}$$

$$t_{min} = \frac{1}{\omega}\left[\tan^{-1}\left(-\frac{1}{\omega\tau_i}\right) + 2\pi\right]. \tag{32b}$$

The corresponding values of the sheath potential are obtained by substituting t_{min} and t_{max} into Eq. (30). In the present analysis, ions crossing the sheath-presheath boundary from the bulk plasma are assumed to be monoenergetic at the Bohm velocity. The ion kinetic energy at the wall is equal to the sum of their initial kinetic energy and the energy they gained moving across the sheath. The latter is equal to $\overline{V}_w$ [Eq. (29)] for the case of a collisionless sheath. Hence,

$$E_{i\,max} = \frac{T_e}{2} + V_{dc} + \frac{V_{ac}}{1+(\omega\tau_i)^2}[\sin(\omega t_{max}) - (\omega\tau_i)\cos(\omega t_{max})], \tag{33a}$$

$$E_{i\,min} = \frac{T_e}{2} + V_{dc} + \frac{V_{ac}}{1+(\omega\tau_i)^2}[\sin(\omega t_{min}) - (\omega\tau_i)\cos(\omega t_{min})]. \tag{33b}$$

The energy dispersion defined as $\Delta E_i = E_{i\,max} - E_{i\,min} = \overline{V}_{max} - \overline{V}_{min}$ is

$$\Delta E_i = \frac{2V_{ac}}{1+(\omega\tau_i)^2}\left\{\cos\left[\tan^{-1}\left(-\frac{1}{\omega\tau_i}\right)+\frac{3\pi}{2}\right] + \omega\tau_i\sin\left[\tan^{-1}\left(-\frac{1}{\omega\tau_i}\right)+\frac{3\pi}{2}\right]\right\}. \tag{34}$$

Depending on the value of $\omega\tau_i$ the above expression can be simplified as follows:

$$\text{Low frequency regime:}\quad \omega\tau_i \ll 1,\quad \Delta E_i \approx 2V_{ac}, \tag{35a}$$

$$\text{High frequency regime:}\quad \omega\tau_i \gg 1,\quad \Delta E_i \approx 2V_{ac}/\omega\tau_i. \tag{35b}$$

Therefore, the energy dispersion of the IED is not a function of the applied frequency when $\omega\tau_i \ll 1$, while at the high frequency regime $\Delta E_i \propto V_{ac}/\omega\tau_i$, a dependence reported in the literature.[16,17]

The ion energy distribution function was calculated based on the observation that the minimum and maximum energy of ions striking the wall correspond to the minimum and maximum values, respectively, of the damped potential at the wall. The range of the damped potential at the wall ($\overline{V}_{max} - \overline{V}_{min}$) was then divided into a large number (normally 500) of intervals $\Delta\overline{V}_w$. For each $\Delta\overline{V}_w$, the corresponding time slot Δt from the known ''damped potential versus time'' waveform was obtained. Since ions enter the sheath with a uniform distribution in phase angles, the number of ions ΔN_i striking the wall is proportional to Δt. The IED function was then obtained by plotting ΔN_i vs ion energy ($\overline{V}_w + kT_e$), where $\overline{V}_w$ is the value of the damped potential at the midpoint of the $\Delta\overline{V}_w$ interval in question.

Figure 7 presents the IED for an argon plasma at different frequencies under otherwise the base case conditions. As the applied frequency is increased the energy dispersion decreases. The low energy peak of the IED is higher than the high energy peak. At very high frequencies, the amplitude of the oscillations of $\overline{V}_w$ is very small and the two peaks of the IED tend to merge. It must be emphasized at this point that the IED depends critically on the sheath potential waveform. This waveform is expected to change as the substrate biasing frequency is varied. In order to predict the shape of the sheath potential waveform, the external circuit supplying power to the electrode has to be considered, along with the rest of the reactor, see for example Ref. 6. In Fig. 7, the same waveform was used (solid line of Fig. 2) for all frequencies. Therefore, Fig. 7 should only be viewed as a qualitative description of the IED as a function of frequency on a biased electrode.

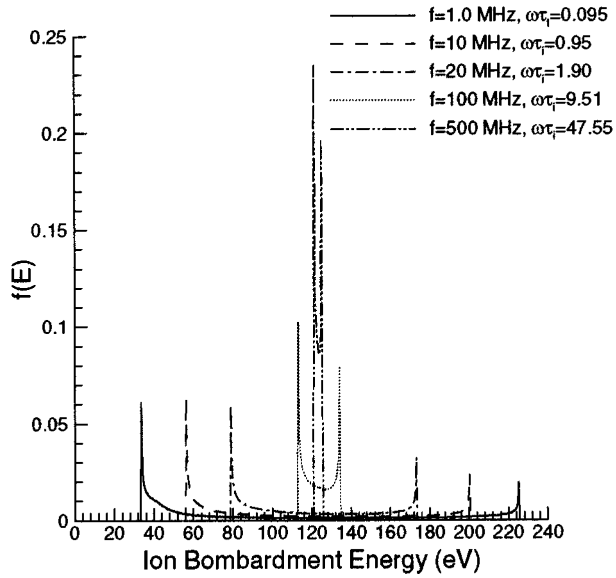

FIG. 7. Ion energy distribution as a function of $\omega\tau_i$. As the value of $\omega\tau_i$ is increased, the energy dispersion is decreased and the IED changes from bimodal to a single peak distribution at very high frequencies. Applied potential is shown as solid line in Fig. 2.

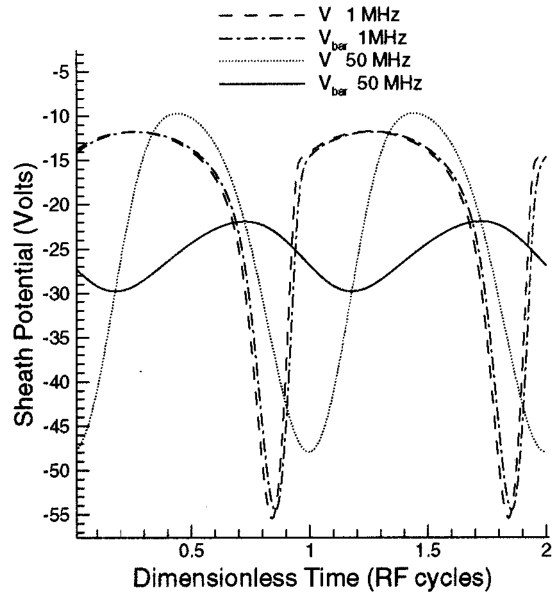

FIG. 8. Waveforms of actual (V) and damped ($V_{\rm bar}$) potential at the electrode as a result of a prescribed sinusoidal current across the sheath. Total current, 30 A/m^2 for a frequency of 1 MHz and 200 A/m^2 for a frequency of 50 MHz. Ion density at sheath edge, $6\times10^{16}\,{\rm m}^{-3}$.

V. CURRENT CONTROL

The previous analysis used a specified potential across the sheath. In this section, the total current flowing through the sheath is specified instead. The total current is the summation of the electron particle current, the ion particle current, and the displacement current,

$$j_e=\frac{1}{4}eu_en_e=\frac{eu_en_s\exp(V/T_e)}{4}, \tag{36}$$

where $u_e=(8eT_e/\pi m_e)^{1/2}$ is the electron thermal velocity,

$$j_i=-en_su_B, \tag{37}$$

$$j_d=\epsilon_0\frac{\partial E}{\partial t}=\epsilon_0\left(\frac{\partial E}{\partial V}\frac{\partial V}{\partial t}+\frac{\partial E}{\partial \overline{V}}\frac{\partial \overline{V}}{\partial t}\right). \tag{38}$$

Equation (27) gives

$$\frac{\partial E}{\partial V}=\frac{1}{E}\frac{en_sT_e}{\epsilon_0}\left\{\frac{M^2}{\overline{V}}\left[\left(1-\frac{2\overline{V}}{M^2T_e}\right)^{1/2}-1\right]+\frac{1}{T_e}\exp\left(\frac{V}{T_e}\right)\right\}, \tag{39}$$

$$\frac{\partial E}{\partial \overline{V}}=\frac{1}{E}\frac{en_sT_e}{\epsilon_0}\frac{M^2V}{\overline{V}^2}\left\{1-\left(1-\frac{2\overline{V}}{M^2T_e}\right)^{1/2}-\frac{\overline{V}}{M^2T_e}\left(1-\frac{2\overline{V}}{M^2T_e}\right)^{-1/2}\right\}. \tag{40}$$

Equations (39) and (40) can be substituted into Eq. (38) to obtain the displacement current in the sheath. Equation (38) can also be used to describe the sheath capacitance. This can be used in equivalent circuits of the plasma reactor[6,22] by which one can calculate the time varying potentials in the system including the plasma and wall potentials.

Assuming a sinusoidal total current through the sheath, $j_{\rm tot}=j_e+j_i+j_d=j_0\sin(\omega t)$, a first-order differential equation for the potential at the electrode V_w is obtained, which is solved numerically along with Eq. (15). The actual and damped sheath potentials are then found, and are shown in Fig. 8 for a low (1 MHz) and a high (50 MHz) frequency case. As before, the damped potential approximates the actual potential at low frequencies and is much reduced in amplitude at high frequencies. Also, the sheath potential is ''clipped'' at low frequencies and is more sinusoidal-like at high frequencies. At low frequencies, when $\omega\tau_i<1$, the sheath is resistive and the displacement current is a small fraction of the total current. At high frequencies, when $\omega\tau_i>1$, the displacement current is a substantial fraction of the total current (Fig. 9).[18] In all cases, the time-average electron current is equal to the positive ion current (constant in our case) ensuring no net charge flow to the electrode over a rf cycle.

A generalized sheath diagram is shown in Fig. 10.[23] Different regimes of operation are shown depending on the ratio ω/ν of the applied field frequency to the ion collision frequency (y axis) and the product $\omega\tau$ of the applied field frequency and the ion transit time through the sheath (x axis). The diagonal ($\nu\tau=1$) separates the collisionless from the collisional sheath regimes. When $\omega\tau<1$, the sheath is resistive, meaning that the ion (and electron) conduction current dominates over the displacement current. On the other hand, for $\omega\tau>1$, the sheath is capacitive, meaning that the displacement current dominates over the ion conduction current. Therefore, four major regimes are shown on the sheath diagram as collisionless resistive, collisionless capacitive, collisional resistive, and collisional capacitive. High density,

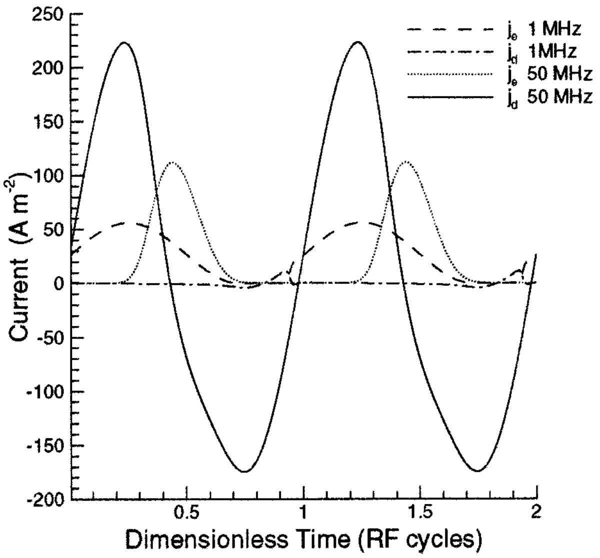

FIG. 9. Temporal behavior of displacement current and electron conduction current for two different applied frequencies. Total current, 30 A/m^2 for a frequency of 1 MHz and 200 A/m^2 for a frequency of 50 MHz. Ion density at sheath edge, $6\times10^{16}\,m^{-3}$.

low pressure plasma reactors with biased rf substrate electrode usually operate in the collisionless-resistive regime. Low density, high pressure capacitively coupled reactors usually operate in the collisional-capacitive regime.

VI. COMPARISON WITH OTHER WORKS

The unified sheath model used in this article has been shown by Riley[20,24] to have the right limiting behavior for very high and very low frequencies. Comparison of the model results with experimental data for intermediate frequencies is difficult because published works do not give all necessary information; for example, the sheath voltage or current waveforms are not provided. For that reason we have chosen to compare the model results with a few theoretical reports that are relevant to the intermediate frequency regime.

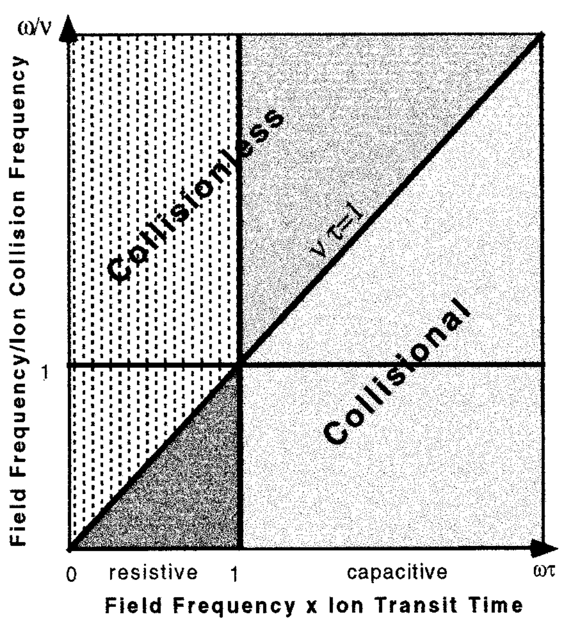

FIG. 10. Generalized sheath diagram for time-dependent sheaths. Different regimes of operation are shown depending on the ratio ω/ν of the applied field frequency to the ion collision frequency (y axis) and the product $\omega\tau$ of the applied field frequency and the ion transit time through the sheath (x axis). The diagonal ($\nu\tau=1$) separates the collisionless from the collisional sheath regimes.

TABLE I. Comparison of the time-average sheath thickness calculated by the model of Barnes *et al.*[a] and the present model.

n_s (m^{-3})	$\omega\tau_i$	Sheath thickness (mm) Barnes *et al.*[a]	Sheath thickness (mm) This work
10^{15}	4.76	3.2	5.05
5×10^{15}	2.13	1.4	2.22
10^{16}	1.50	1.0	1.55
5×10^{16}	0.67	0.44	0.70
10^{17}	0.48	0.32	0.52
5×10^{17}	0.21	0.14	0.29
10^{18}	0.15	0.10	0.23

[a]See Ref. 12.

Barnes *et al.*[12] used Lieberman's model[3] to calculate the sheath thickness of an argon discharge at $f=5$ MHz with $T_e=5$ eV. Table I gives the time-average sheath thickness found by Barnes *et al.* and by the sheath model reported in this article for a range of plasma densities at the sheath edge. The agreement between the two models is reasonable. Lieberman's model is valid when $\omega\tau_i \gg 1$. This is the reason the relative error between the two models increases as the product $\omega\tau_i$ is decreased. Also, the calculated sheath thickness depends on the value used for the electric field at the sheath-presheath interface, Eq. (20). A larger value of E_s gives a smaller sheath thickness.

Flender and Wiesemann[25] measured the ion energy distribution of an argon plasma at 13.56 MHz. For an applied voltage (estimated) of $V_w=-220-212\sin(\omega t)$, $T_e=5$ eV, and $n_s\approx1.17\times10^{15}\,m^{-3}$, they measured an energy dispersion of about 40 eV. For another set of conditions, $V_w=-87.8-79.95\sin(\omega t)$, $T_e=3.9$ eV, and $n_s\approx3.95\times10^{14}\,m^{-3}$, the energy dispersion was found to be about 10 eV. The present model predicted for the first set of conditions $\Delta E_i=46.2$ eV, and for the second $\Delta E_i=10.0$ eV. The agreement is fairly good taking into account the experimental uncertainty in determining the electron temperature and plasma density.

Finally, Nitschke and Graves[26] used the Godyak–Sternberg sheath model[4] along with a plasma fluid model to predict the discharge behavior. For the case of an argon plasma under the conditions of bulk density $n_0=1.39\times10^{18}\,m^{-3}$, $T_e=2.19$ eV, $f=1.59$ MHz, and $j_{tot}=300\,A/m^2$, they found a time-average sheath thickness of 180 μm. The present model predicted a time-average sheath thickness of 175 μm for the same conditions.

VII. CONCLUSIONS

The unified sheath model of Miller and Riley[6] has been used to solve for the spatiotemporal profiles of important sheath variables such as the actual potential, the damped potential to which ions respond, ion and electron densities, sheath thickness and capacitance, and ion transit time. The model requires as input the electron (ion) density and electron temperature at the sheath edge, and the waveform of either the sheath voltage or the total current passing through the sheath. While the vast majority of sheath models published to date are applicable to either very high or very low frequencies (actually either very high or very low values of $\omega\tau_i$), the present model is applicable throughout the rf frequency range from 10 s of kHz to 100 s of MHz. The full numerical solution of the coupled sheath model equations verified that the damped potential is linearly dependent on the actual potential, where the proportionality constant is a function of time only. Based on this observation the sheath equations can be decoupled and semianalytical solutions for the sheath variables obtained. In addition, an analytic expressions was derived for the energy dispersion of the bimodal IED. Model results were in reasonable agreement with the few published works covering the intermediate frequency regime.

Currently there is much interest in multidimensional plasma reactor simulations.[22,27] Resolving the thin plasma sheath in such simulations is impractical due to the vast disparity in length scales between the reactor and the sheath. It then becomes necessary to splice a sheath model to the reactor simulation. Semianalytic sheath models such as that described in the present work can be particularly useful for these applications.

ACKNOWLEDGMENTS

Thanks are due to M. Riley and V. I. Kolobov for helpful discussions. This work was supported financially by the National Science Foundation (CTS-9713262) and the State of Texas through the Texas Advanced Technology Program.

[1] M. A. Lieberman and A. J. Lichtenberg, *Principles of Plasma Discharges And Materials Processing* (Wiley, New York, 1994).
[2] E. Kawamura, V. Vahedi, M. A. Lieberman, and C. K. Birdsall (unpublished).
[3] M. A. Lieberman, IEEE Trans. Plasma Sci. **16**, 638 (1988).
[4] V. A. Godyak and N. Sternberg, Phys. Rev. A **42**, 2299 (1990).
[5] A. Metze, D. W. Ernie, and H. J. Oskam, J. Appl. Phys. **60**, 3081 (1986).
[6] P. A. Miller and M. E. Riley, J. Appl. Phys. **82**, 3689 (1997).
[7] K. U. Riemann, Phys. Plasmas **4**, 4158 (1997).
[8] W. J. Goedheer and P. M. Meijer, IEEE Trans. Plasma Sci. **19**, 245 (1991).
[9] R. T. Farouki, S. Hamaguchi, and M. Dalvie, Phys. Rev. A **45**, 5913 (1992).
[10] R. T. C. Tsui, Phys. Rev. **168**, 107 (1968).
[11] M. J. Kushner, J. Appl. Phys. **58**, 4024 (1985).
[12] M. S. Barnes, J. C. Foster, and J. H. Keller, IEEE Trans. Plasma Sci. **19**, 240 (1991).
[13] A. D. Richards, B. E. Thompson, and H. H. Sawin, Appl. Phys. Lett. **50**, 492 (1987).
[14] D. P. Lymberopoulos and D. J. Economou, J. Vac. Sci. Technol. A **12**, 1229 (1994).
[15] T. Makabe, N. Nakano, and Y. Yamaguchi, Phys. Rev. A **45**, 2520 (1992).
[16] P. Benoit-Cattin and L. C. Bernard, J. Appl. Phys. **39**, 5273 (1968).
[17] Y. Okamoto and H. Tamagawa, J. Phys. Soc. Jpn. **29**, 187 (1970).
[18] J. W. Coburn and E. Kay, J. Appl. Phys. **43**, 4965 (1972).
[19] V. I. Kolobov and D. J. Economou, Appl. Phys. Lett. **72**, 656 (1998).
[20] M. E. Riley, Sandia National Laboratories Technical Report SAND96-1948 UC-401, 1996.
[21] A. C. Hindmarsh, LBL Report No. UCRL-87406, 1982 and No. UCRL-89311, 1983.
[22] S. Rauf and M. J. Kushner, J. Appl. Phys. **83**, 5087 (1998).
[23] V. I. Kolobov and D. J. Economou (unpublished).
[24] M. E. Riley, Sandia National Laboratories Technical Report SAND95-0775 UC-401, 1995.
[25] U. Flender and K. Wiesemann, J. Phys. D: Appl. Phys. **27**, 509 (1994).
[26] T. E. Nitschke and D. B. Graves, IEEE Trans. Plasma Sci. **23**, 717 (1995).
[27] D. J. Economou, J. Feldsien, and R. S. Wise, in *Electron Kinetics and Applications of Glow Discharges*, edited by U. Kortshagen and L. D. Tsendin (Plenum, New York, 1998).